JOURNAL OF SOLID STATE CHEMISTRY **137,** 185–190 (1998)
ARTICLE NO. SC977631

Hydrothermal Synthesis and Characterization of Nanocrystalline γ-Fe_2O_3 Particles

Dairong Chen*,† and Ruren Xu†,[1]

*Department of Chemistry, Shandong University, Jinan 250100, China and †Department of Chemistry, Jilin University, Changchun 130023, China

Received March 20, 1997; in revised form September 16, 1997; accepted September 19, 1997

The γ-Fe_2O_3 particles with nanometer size have been hydrothermally synthesized using 2-methoxyethanol (MOE)-H_2O mixed solvent and acetylacetone(Hacac) as additive from iron(II) 2-methoxyethoxides ($Fe(MOEO)_2$). The typical reaction conditions are as follows:

reaction temperature	**140°C**
reaction time	**7–10 days**
$Fe(MOEO)_2$ content	**0.28 mol dm^3**
molar ratio of MOE/H_2O	**0.4**
molar ratio of Hacac/$Fe(MOEO)_2$	**1.2 ~ 2.0**

The as-prepared powders are characterized by experimental techniques such as IR, XRD, TG-DTA, and TEM. The magnetic properties of the particles have been evaluated using a vibrating magnetometer. The nanocrystalline γ-Fe_2O_3 particles appear at a lower agglomeration and phase transformation temperature than those prepared from other methods.

INTRODUCTION

Many magnetic recording media have been intensively studied due to the increased need for high area density (1–3). Of the particulate media, γ-Fe_2O_3 powders have been widely used for the longest period of time because of their excellent ferromagnetic properties, and they continue to be very important for many applications (4, 5). The conventional process for the preparation of γ-Fe_2O_3 powders is the controlled oxidation of Fe_3O_4. The mean size of the final particles usually range in micrometer (6). Using the hydrothermal method, Blesa *et al.* (7) have also prepared γ-Fe_2O_3 powders with micrometer size from sodium orthoferrite.

In recent years, there have been some papers on the synthesis of γ-Fe_2O_3 particles with nanometer-size having potential applications for ferrofluid, magnetic refrigeration, bioprocessing, and information storage (8–14). Ziolo *et al.* (9, 12) reported the matrix-mediated synthesis of γ-Fe_2O_3 nanocrystallites in aqueous solution using $FeCl_24H_2O$ as raw material. Chhabra *et al.* (8) have also prepared nanocrystalline γ-Fe_2O_3 particles from a microemulsion-mediated reaction. However, these powders were all derived from aqueous solution containing some inorganic ions such as Na^+ and Cl^-, which tended to be a major source of contamination of these particles (15).

In the last decade, a variety of powders have been prepared by the hydrothermal method. It is regarded as superior to other methods for certain reasons (16). To obtain crystalline particles with a single phase, a mineralizer is usually necessary, and the products are likely to be contaminated by the mineralizer (17). In this paper, we report the hydrothermal synthesis of γ-Fe_2O_3 particles with nanometer-size in 2-methoxyethanol (MOE)-H_2O mixed solvent from iron(II) 2-methoxyethoxides ($Fe(MOEO)_2$). This method has the advantage that the resultant precipitates are not contaminated, because the organic solution having a lower dielectric constant is free from ionic species. The purpose of this paper is to find suitable conditions for the preparation of pure γ-Fe_2O_3 nanocrystallites and to characterize the as-prepared powders in detail. Some metastable materials such as zeolites (18, 19) can be hydrothermally synthesized from non-aqueous solution (i.e., organic solvothermal process) at a lower temperature through this process, and metal oxides with a stable phase have been prepared at higher temperatures in previous work (20, 21).

EXPERIMENTAL

Synthesis

All the reagents were of analytical grade, purchased from Shanghai Chemical Co. (China) and further purified to dehydrate using 4A molecular sieve and CaH_2 (22) before utilization. $Fe(MOEO)_2$ used in this work was prepared in our laboratory according to the method described in

[1]To whom correspondence should be addressed.

0022-4596/98 $25.00

Ref. 23. The reaction was represented as Eq. [1]:

$$FeCl_2 + MOE + NH_3 \xrightarrow[N_2\ \text{atmosphere}]{\text{refluxing}} Fe(MOEO)_2 + NH_4Cl\downarrow. \quad [1]$$

The by-product ammonium chloride in Eq. [1] was discarded by filtration in N_2 atmosphere and the filtrate was distilled under reduced pressure, then the resident was further purified by extraction with purified benzene (The final product: Anal. Fe 27.06, C 35.10, H 6.92%; Cal. Fe 27.10, C 34.98, H 6.85%). An amount of $Fe(MOEO)_2$ was added to the flask containing some MOE, and the solution was refluxed for 4 h at 140°C under a flow of N_2. A given amount of acetylacetone (Hacac) was dropped into the above solution and refluxing was continued for an additional 2 h. A mixed solvent in which molar ratio of MOE/H_2O ranged from 0.05–0.1 was added dropwise under electromagnetic stirring. Next, 25.0 cm^3 of colloid solution was poured into a 30.0 cm^3 stainless steel autoclave with a Teflon liner and reacted at a specified temperature and time, then the autoclave was cooled to room temperature. The precipitate was obtained by centrifugation, washed with acetone, and dried overnight under N_2 atmosphere at ambient temperature.

Characterization

The as-synthesized samples were characterized by X-ray diffraction (XRD) patterns obtained on a Rigaku D/Max-γA diffractometer using Cu$K\alpha$ as incident radiation ($\lambda = 1.5418$ Å, 40 mA, 80 KV). The XRD intensity data were collected over the range $20 < 2\theta < 70^\circ$ at room temperature. The mean size and morphologies of γ-Fe_2O_3 particles were observed by transmission electron microscopy (TEM, JEM-100CXII). The thermogravimetric (TG) and differential thermal analysis (DTA) results were recorded on a Perkin-Elemer TG-700 and DTA-7000 spectrometer. All TG measurements were performed in a platinum container in an air flow. Heating was carried out from 20 to 640°C at a rate of 10°C/min. A vibrating sample magnetometer (VSM-9500) was used to evaluate the magnetic properties at room temperature.

RESULTS AND DISCUSSION

It was necessary to find suitable $Fe(MOEO)_2$ content in solution for preparing the planned product in the hydrothermal process. Table 1 shows the product with varying $Fe(MOEO)_2$ content while other conditions are held constant. The $Fe(MOEO)_2$ content had an important influence on the product. Higher $Fe(MOEO)_2$ content gave Fe_3O_4 and amorphous precipitate, while lower $Fe(MOEO)_2$ content resulted in the formation of β-FeOOH or α-Fe_2O_3. The typical $Fe(MOEO)_2$ content was 0.28 mol dm^{-3} for the synthesis of γ-Fe_2O_3.

TABLE 1
Product with Varying $Fe(MOEO)_2$ Content

Sample	$Fe(MOEO)_2$ content (mol dm^{-3})	Product
1	0.15	β-FeOOH + γ-Fe_2O_3
2	0.28	γ-Fe_2O_3
3	0.40	γ-Fe_2O_3 + Fe_3O_4
4	0.60	Fe_3O_4
5	0.90	Fe_3O_4 + amorphous precipitate

Note: reaction temperature: 140°C, reaction time: 7 days, molar ratio of Hacac/$Fe(MOEO)_2$: 1.5, molar ratio of MOE/H_2O : 0.4.

Dubois and Demazean have confirmed that solvent affected the product (20). For the mixed solvent its property would vary with increasing or decreasing molar ratio of MOE/H_2O. The products are listed in Table 2 corresponding to different MOE content in the mixed solvent. Higher MOE content, i.e., higher molar ratio of MOE/H_2O, led to the formation of Fe_3O_4 or amorphous precipitate, and lower MOE content gave β-FeOOH. The suitable molar ratio of MOE/H_2O was 0.4 for the preparation of γ-Fe_2O_3.

The above results demonstrated that suitable Fe $(MOEO)_2$ content and molar ratio of MOE/H_2O in solution would be necessary for the formation of γ-Fe_2O_3. MOE has lower dielectric constant and vapor pressure than water. With increasing MOE content, the oxidation of the mixed solvent would be expected to decrease due to corresponding water content being lowered. With the mixed solvent and reaction temperature fixed, the oxidation of the solvent would hold constant. Thus, higher $Fe(MOEO)_2$ content might result in imperfect hydrolysis and oxidation of Fe(II), and lower $Fe(MOEO)_2$ content would lead to the perfect oxidation of Fe(II). Lower MOE content would bring about higher vapor pressure and give the stable phase α-Fe_2O_3.

TABLE 2
Product with Varying Molar Ratio of MOE/H_2O in Mixed Solvent

Sample	Molar ratio of MOE/H_2O	Product
6	0.0	β-FeOOH + α-Fe_2O_3
7	0.2	β-FeOOH + γ-Fe_2O_3
2	0.4	γ-Fe_2O_3
8	0.6	γ-Fe_2O_3 + Fe_3O_4
9	1.0	Fe_3O_4 + amorphous precipitate
10	2.0	amorphous precipitate

Note: reaction temperature: 140°C, reaction time: 7 days, molar ratio of Hacac/$Fe(MOEO)_2$: 1.5, $Fe(MOEO)_2$ content: 0.28 mol dm^{-3}.

TABLE 3
Effect of Hacac on the Product

Sample	Molar ratio of Hacac/$Fe(MOEO)_2$	Product
11	4.0	amorphous precipitate
12	3.0	$Fe_3O_4 + \gamma$-Fe_2O_3
13	2.4	$Fe_3O_4 + \gamma$-Fe_2O_3
2	1.5	γ-Fe_2O_3
14	0.5	α-FeO_3

Note: reaction temperature: 140°C, reaction time: 7 days, $Fe(MOEO)_2$ content: 0.28 mol dm^{-3}, molar ratio of MOE/H_2O: 0.4.

If the preparation of γ-Fe_2O_3 particles were only considered to be the product of hydrolysis and oxidation of Fe(II), the overall formation process might be represented as:

$$Fe(MOEO)_2 \xrightarrow[\text{refluxing}]{\text{Hacac}} Fe(acac)_x(MOEO)_{2-x}$$

$$\xrightarrow[\text{hydrothermal condition}]{H_2O} Fe(OH)_2 \xrightarrow[\text{hydrothermal condition}]{O_2} \gamma\text{-}Fe_2O_3.$$

Here, the hydrolysis rate of $Fe(acac)_x(MOEO)_{2-x}$ was slower than that of $Fe(MOEO)_2$ because of the chelation of Hacac (23). The hydrolysis of $Fe(acac)_x(MOEO)_{2-x}$ and transformation of $Fe(OH)_2$ to γ-Fe_2O_3 were accelerated by heating, and the latter was capable of taking place through intermediates such as FeO(OH) and Fe_3O_4 (9). Regardless of the formation mechanism of γ-Fe_2O_3, it was apparent that a suitable amount of Hacac was necessary.

After it was seen that Hacac affected the product, subsequent experiments were carried out. Table 3 shows the products with varying Hacac contents while other conditions are held constant. It indicates that the presence of a small amount of Hacac resulted in amorphous precipitate or some crystalline phases other than γ-Fe_2O_3. When the molar ratio of Hacac/$Fe(MOEO)_2$ was greater than 4.0, unknown amorphous precipitate formed. IR analysis demonstrated that the amorphous precipitate contained $acac^-$, which was probably a partial hydrolytic product of the chelate intermediate. When the molar ratio of Hacac/Fe $(MOEO)_2$ ranged from 2.4 to 3.0, a mixture of Fe_3O_4 and γ-Fe_2O_3 was produced. But insufficient Hacac (molar ratio of Hacac/MOE lower than 0.5), resulted in the formation of α-Fe_2O_3. The typical molar ratio of Hacac/$Fe(MOEO)_2$ was 1.2–2.0 for the preparation of γ-Fe_2O_3 particles with a single phase. The effect of Hacac might be explained: (1) the formation of γ-Fe_2O_3 was on the basis of the oxidation and hydrolysis of Fe(II), (2) the γ-Fe_2O_3 phase was metastable and would transform to the stable phase α-Fe_2O_3, (3) the formation and phase transformation of γ-Fe_2O_3 included thermodynamics and dynamic processes which were subject to the reaction conditions. The hydrolysis and oxidation of $Fe(acac)_x(MOEO)_{2-x}$ was the first course of the hydrothermal reaction. Its rate might affect the product. Varying molar ratios of Hacac/$Fe(MOEO)_2$ resulted in a variety of values for x in $Fe(acac)_x(MOEO)_{2-x}$, and the hydrolytic rate of the intermediate varied. Thus, varying molar ratios of Hacac/$Fe(MOEO)_2$ led to the formation of varying products.

For any hydrothermal process, the effects of reaction temperature and time on product cannot be ignored. First, reaction temperature was investigated. Table 4 reveals that (when the temperature was lower than 100°C), the product contained amorphous precipitate and Fe_3O_4 other than γ-Fe_2O_3. When reaction temperature was raised to 120°C, γ-Fe_2O_3 appeared and amorphous precipitate disappeared. When the temperature was increased to 140°C, γ-Fe_2O_3 particles with a single phase were precipitated. As the reaction temperature was increasingly raised, γ-Fe_2O_3 content in the product decreased and α-Fe_2O_3 was produced. When the temperature was increased to above 180°C, γ-Fe_2O_3 disappeared and the monolithic α-Fe_2O_3 formed. This was because higher temperature resulted in increasing the oxidation of the mixed solvent as well as oxygen dissolved in the solution.

To study reaction time, the hydrothermal reaction was held at 140°C for varying lengths of time. XRD patterns in Fig. 1 show that reaction time as long as 6 days was necessary to form γ-Fe_2O_3 (sample 19); 7 days was necessary for preparing γ-Fe_2O_3 powders with a single phase (sample A). After reaction for 10 days, the product remained the same phase (sample B). Compared to those of sample A, the XRD peak intensity of sample B increased and the d(222) peak appeared. However, by prolonging reaction time to 14 days, α-Fe_2O_3 was produced due to the phase transformation of γ-Fe_2O_3 (sample 20). After continued prolonging to 20 days, γ-Fe_2O_3 disappeared and the crystalline phase in product was only α-Fe_2O_3 (sample 21). Figure 1 also reveals that the XRD pattern (d311) peak of γ-Fe_2O_3 became sharper and the width of midpeak became smaller with the prolonging of reaction time, which demonstrates that the particles grew larger.

TABLE 4
Effect of Reaction Temperature on the Product

Sample	Reaction temperature (°C)	Product
15	90	amorphous precipitate
16	120	$Fe_3O_4 + \gamma$-Fe_2O_3
2	140	γ-Fe_2O_4
17	160	γ-$Fe_2O_3 + \alpha$-Fe_2O_3
18	180	α-Fe_2O_3

Note: reaction time: 7 days, $Fe(MOEO)_2$ content: 0.28 mol dm^{-3}, molar ratio of MOE/H_2O: 0.4, molar ratio of Hacac/$Fe(MOEO)_2$: 1.5.

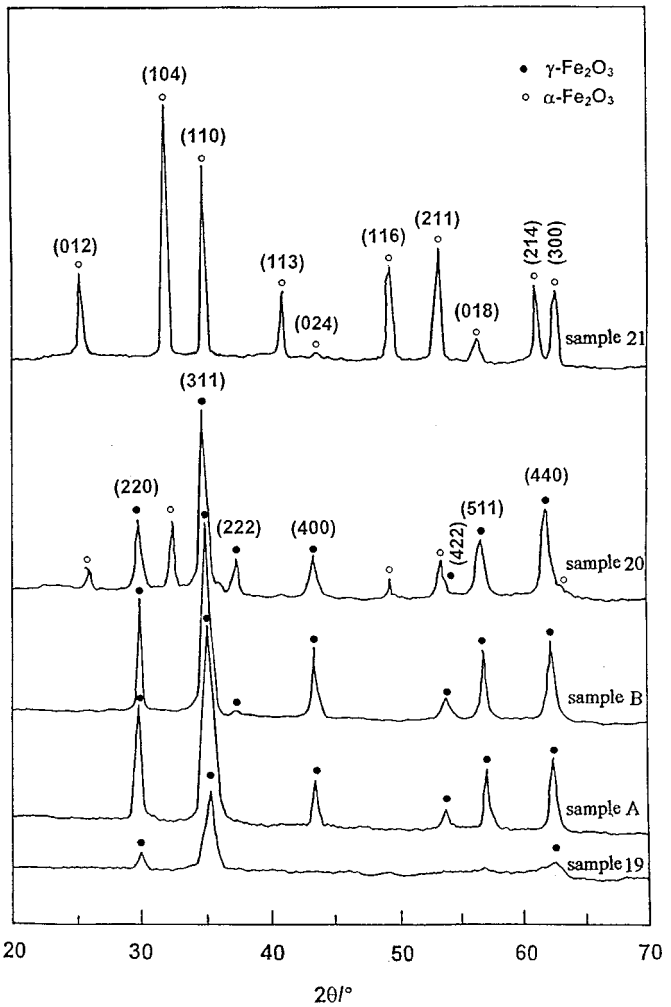

FIG. 1. XRD patterns of the products with varying reaction times while other conditions held constant (reaction temperature: 140°C, $Fe(MOEO)_2$ content: 0.28 mol dm^{-3}; molar ratio of MOE/H_2O: 0.4, molar ratio of $Hacac/Fe(MOEO)_2$: 1.5, reaction time for sample 19: 3 days, sample A: 7 days, sample B: 10 days, sample 20: 14 days, sample 21: 20 days).

To investigate the effects of reaction conditions on the products and particle size on the product properties, sample A (same as sample 2 in tables) and sample B (its synthesis conditions as well as those of sample A were denoted in Fig. 1) were applied to characterize in detail. Figure 2 shows TEM micrographs of the above samples. All the particle morphologies appeared polyhedral. The γ-Fe_2O_3 particles were nearly equiaxed with 16–18 nm for sample A and 20–28 nm for sample B, respectively. The particle size of sample B was larger than that of sample A, indicating that particle size increased with the prolonging of reaction time.

The considerable line-broadening of XRD patterns for sample A and B (see Fig. 1) also demonstrates the nanocrystallite nature of γ-Fe_2O_3 powders. Using well known Scherre's equation calculated from X-ray line (d311) broadening, the particle size of sample A was 8–12 nm and sample B was 16–26 nm. γ-Fe_2O_3 particles prepared by the hydrothermal process showed lower agglomeration compared with the spray pyrolysis method (24). One factor was that the mixed solvent had lower dielectric constant than water and decreased the surface energy of the grains (25); another was that spray pyrolysis included a higher-temperature process. IR spectra of all samples in Fig. 3 show three distinguishing adsorption bands at 1420, 1620, and 3440 cm^{-1} under room temperature, except three bands at 627, 566, and 427 cm^{-1} for sample A (see a in Fig. 3) and three bands at 643, 582, and 436 cm^{-1} for sample B (see b in Fig. 3) which were attributed to the characteristic of disordered γ-Fe_2O_3 (8, 10). The characteristic adsorption bands of sample A were on a lower wavenumber compared to those of sample B due to its smaller particles. The band at 1420 cm^{-1} was attributed to the stretching vibration of N_2, and two bands at 3440 and 1620 cm^{-1} were due to characteristic IR spectra of H_2O molecular adsorbed on the surface of γ-Fe_2O_3 particles. When the samples were heated to 120°C, the adsorption bands at 1420 cm^{-1} weakened because of the desorption of nitrogen from the surface of

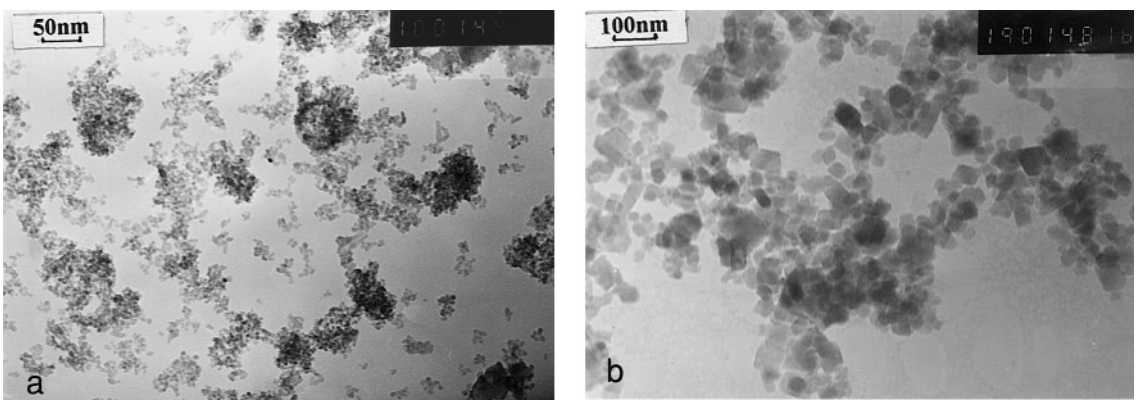

FIG. 2. TEM micrographs of (a) sample A and (b) sample B.

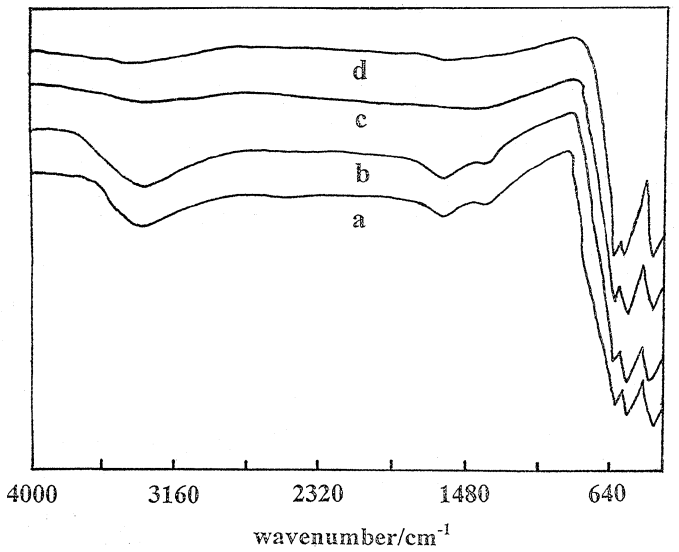

FIG. 3. IR spectra of (a) sample A at room temperature, (b) sample B at room temperature, (c) sample A at 120°C, and (d) sample B at 120°C.

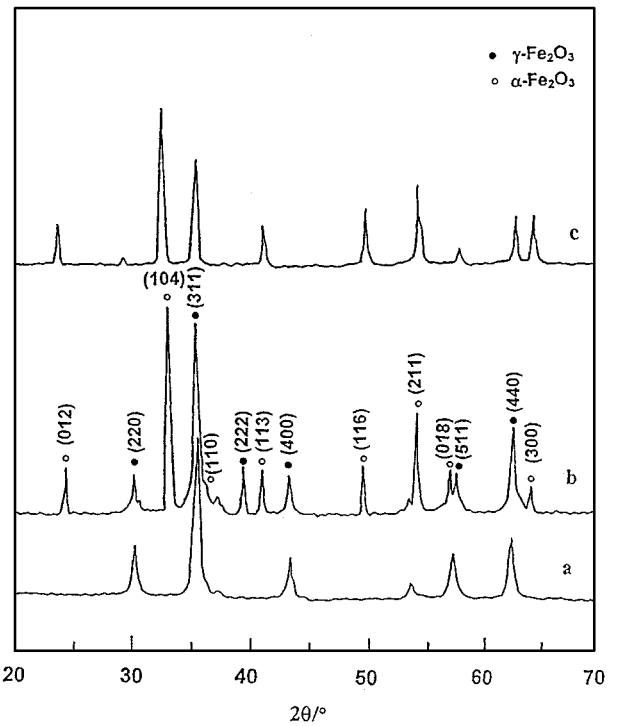

FIG. 5. XRD patterns of sample A at (a)100°C, (b) 400°C, and (c)550°C.

γ-Fe_2O_3 particles and the bands on 3440 and 1620 cm^{-1} changed to feeble (c and d in Fig. 3). The TG-DTA data for the γ-Fe_2O_3 particles are shown in Fig. 4. It shows an exothermic peak centered at 400°C for sample A (a in Fig. 4) and at 420°C for sample B (b in Fig. 4) on the corresponding DTA curve, but no distinguishing variation in weight on the TG curves. This was due to the phase transformation of γ-Fe_2O_3: γ-$Fe_2O_3 \rightarrow \alpha$-$Fe_2O_3$. The above phase transformation was confirmed by the XRD patterns of sample A at varying temperatures in Fig. 5. This phase transformation temperature was lower than the reported values (26–28). It was known that the temperature was subject to the particle size for any powder. For the nanocrystalline powders, the temperature would decrease with decreasing mean size of particles. Thus, the phase transformation temperature of sample A was lower than that of sample B. Figure 4 reveals that for temperatures 130–240°C, there was a weight loss of less than 1.0%, but the corresponding DTA curve exhibited no distinguishing variation. These results are probably explained by the loss of solvent absorbing on the surface γ-Fe_2O_3 particles. From the TG-DTA data, there was no evidence that the γ-Fe_2O_3 particles were contaminated by the starting organic materials. This result was consistent with that of IR analysis.

Magnetic characterization of the γ-Fe_2O_3 particles was done at room temperature. Hysteresis measurements were made with a field scan of ± 2.0 KOe (see Fig. 6). The

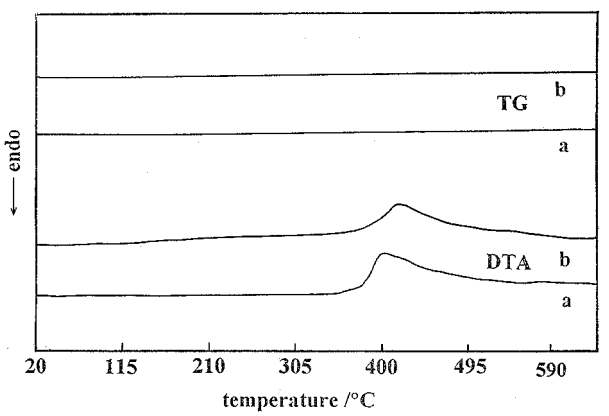

FIG. 4. TG-DTA curves of (a) sample A and (b) sample B.

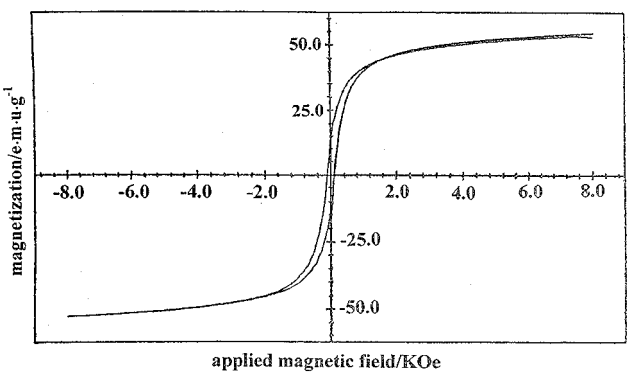

FIG. 6. The hysteresis measurements of sample A in Table 5.

TABLE 5
Magnetic Properties of Nanocrystalline γ-Fe_2O_3 Particles

Sample	Saturation magnetization	Coercivity	Magnetizability
	moment (emu g^{-1})	(KAm^{-1})	(emu g^{-1})
A	52.78	12.33	12.58
B	72.87	19.79	17.54

Note: measuring temperature: $25.0 \pm 0.5^{\circ}C$, measuring time: 323 s, magnetic density: 8000 Oe.

corresponding values are listed in Table 5. The lower saturation magnetization moment and coercivity values were due to the presence of super paramagnetization (29, 30). However, the corresponding values of sample A were lower than those of sample B due to its smaller particles.

ACKNOWLEDGMENTS

The authors thank Professor X. H. Ding of the Physics Department, Shandong University, for the measurement of magnetic properties. Thanks are also due to Mr. J. Huang, who performed the XRD work at the Analytical Centre, Shandong University.

REFERENCES

1. H. L. Luo and G. H. Wang, *J. Magn. Magn. Mater*. **129,** 389 (1994).
2. K. J. Davis, S. Wells, R. V. Upadhyay, S. W. Chares, K. O'Grady, M. El-Hilo, T. Meaz, and S. Morup, *J. Magn. Magn. Mater*. **149,** 14 (1995).
3. R. Ao, L. Kummerl, and D. Haarer, *Adv. Mater*. **7,** 495 (1995).
4. N. Takahashi, N. Kakuda, A. Ueno, K. Yamaguchi, and T. Fujii, *Jpn. J. Appl. Phys*. **28,** 244 (1987).
5. H. E. Jones, P. R. Bissell, and R. W. Chantrell, *J. Magn. Magn. Mater*. **83,** 445 (1990).
6. C. Wang and J. Chen, *Bull. Chin. Sci*. **38,** 1947 (1993).
7. M. C. Blesa, E. Moran, N. Nenendez, J. D. Tornero, and C. Torron, *Mater. Res. Bull*. **28,** 837 (1993).
8. V. Chhabra, P. Ayyub, S. Chattopadhyay, and A. N. Maitra, *Mater. Lett*. **26,** 21 (1996).
9. R. F. Ziolo, E. P. Giannclis, B. A. Weinstein, M. P. O. Horo, B. N. Ganguly, V. Mehrotra, M. W. Russell, and D. R. Huffman, *Science* **257,** 219 (1992).
10. T. Gonzalez-Carreno, A. Mifsud, J. M. Palacios, and C. J. Serna, *Mater. Chem. Phys*. **27,** 287 (1991).
11. K. Suresh and K. C. Patil, *J. Mater. Sci. Lett*. **12,** 572 (1993).
12. E. Kroll, F. M. Winnik, and R. F. Ziolo, *Chem. Mater*. **8,** 1594 (1996).
13. W. Chang, M. Deng, T. Tsai, and T. Ching, *Jpn. J. Appl. Phys*. **31,** 1343 (1992).
14. Y. S. Kang, S. Risbud, J. F. Rabolt, and P. Stroeve, *Chem. Mater*. **8,** 2209 (1996).
15. Y. Konishi, T. Kawamura, and S. Asai, *Ind. Eng. Chem. Res*. **32,** 2888 (1993).
16. R. Vivekanadan, S. Philip, and T. R. N. Kutty, *Mater. Res. Bull*. **22,** 99 (1986).
17. K. Kukuta, A. Tosa, T. Yogo, and S. Hirano, *Chem. Lett*. 2267 (1994).
18. D. M. Bibby and M. P. Dale, *Nature* **317,** 157 (1985).
19. Q. Huo and R. Xu, *J. Chem. Soc., Chem. Commun*. 1391 (1992).
20. T. Dubois and G. Demazeau, *Mater. Lett*. **19,** 38 (1994).
21. D. W. Matson, J. C. Linehan, and R. M. Bean, *Mater. Lett*. **14,** 222 (1992).
22. D. F. Shriver and M. A. Drezden, "The Manipulation of Air-Sensitive Compounds," 2nd ed., Wiley–Interscience, New York, 1986.
23. D. C. Bradley, R. C. Mehrotra, and D. P. Gaur, "Metal Alkoxide," Academic Press, London, 1978.
24. T. Gonzlalez-Carreno, M. P. Morals, M. Gracia, and C. J. Serna, *Mater. Lett*. **18,** 151 (1993).
25. J. H. Jean and T. A. Ring, *Am. Ceram. Soc. Bull*. **65,** 1574 (1984).
26. R. Gomez-Villacieros, L. Hernan, J. Morales, and J. L. Tirado, *Mater. Res. Bull*. **22,** 513 (1987).
27. R. M. T. Sanchez, *J. Mater. Sci. Lett*. **15,** 461 (1996).
28. Y. Yamagnchi, K. Matsumoto, and T. Fujii, *Jpn. J. Appl. Phys*. **30,** 478 (1991).
29. D. J. Craik, "Magnetic Oxides," Wiley, New York, 1975.
30. D. L. Leslie-Pelecky and R. D. Rieke, *Chem. Mater*. **8,** 1770 (1996).